Aust. J. Phys., 1979, **32**, 261–77

Models of Radio Recombination Line Sources

M. J. Batty

School of Physics, University of Sydney, Sydney, N.S.W. 2006;
present address: Jet Propulsion Laboratory, 4800 Oak Grove Drive, Pasadena, California 91103, U.S.A.

Abstract

Models for the southern HII regions RCW 38, RCW 49, the Carina Nebula, G305+0 and M17 are constructed using a range of line and continuum data. Electron temperatures in the range 5000–7300 K are derived from the analysis, and in most cases these are consistent with estimates obtained from radio continuum measurements. The presence of a low temperature ($\leqslant$4000 K) outer region in RCW 38 is suggested by the low frequency line data. Density inhomogeneities are found to be significant in all sources, while the predicted line widths are consistent with an observed lack of collisional broadening at low frequencies.

1. Introduction

Our current understanding of the physical conditions in gaseous nebulae has been aided by the use of radiofrequency recombination lines as probes of nebular electron temperature and density. In particular, it has been possible to interpret a wide range of recombination line and radio continuum data in terms of models with nonuniform electron density structure (e.g. Brocklehurst and Seaton 1972; Cato 1973; Lockman and Brown 1975). These models generally have the following characteristics: (i) a uniform, or near-uniform, electron temperature; (ii) spherical symmetry; (iii) a centrally peaked electron density distribution.

The interpretation of nebular radio recombination lines has been concentrated on northern HII regions (mainly the Orion Nebula) due to the availability of observational data. However, recombination line data covering a wide frequency range, from $\sim$8·9 GHz (H90α) to $\sim$0·4 GHz (H252α), have become available for several bright southern HII regions. The present analysis is based on these data. Models have been constructed for five southern HII regions: RCW 38, RCW 49, the Carina Nebula, G305+0 and M17, and the work described here represents the first systematic analysis of available recombination line data for the first four of these objects.

An attempt has been made to develop a consistent procedure for defining those model properties which feature prominently in low frequency recombination line behaviour. Below $\sim$1 GHz, the major contribution to the apparent line emission usually arises in the outer low-density regions of the nebulae, rather than in the central denser parts, since the line radiation from the denser regions is highly collisionally broadened. It is difficult to determine the electron density in the outer regions from continuum spectra or line data alone. However, data from radio continuum maps often allow the determination of r.m.s. electron densities to large

distances from the centres of bright nebulae. In the present analysis, high frequency radio continuum maps are used to model the overall density structure. The electron temperature and the local density fluctuations are then allowed to vary until good agreement is obtained with the recombination line observations. Using this method, it has been possible to infer volume-averaged electron temperatures, electron density fluctuations and, in RCW 38, the presence of a radial temperature variation.

2. Recombination Line Data

The recombination line data used in the analysis are now briefly reviewed. The northernmost nebula, M17, has been studied most intensely, whilst observations of the other four sources, all made with the Parkes radiotelescope, have produced far less data. Used in the analysis were the line data summarized by Hjellming and Gordon (1971), together with measurements by McGee and Gardner (1968), McGee *et al.* (1969), Gardner *et al.* (1970*a*, 1970*b*), Simpson (1970), Wilson *et al.* (1970), Pedlar and Davies (1972), Waltman and Johnston (1973), Batty (1974), Gordon *et al.* (1974), Huchtmeier (1974) and McGee *et al.* (1975).

Typical observational uncertainties in line to continuum ratios are $\sim 10\%$. Whenever the original authors quoted only a value of $T_L \Delta v / T_c$ (where Δv, T_L and T_c are the half-power line width, and the line and the continuum temperatures respectively), I have calculated the integrated line to continuum ratio $\int T_L \, dv / T_c$ by assuming a gaussian line shape, since the observed line parameters were usually obtained by gaussian fitting. The intensities of the H113β and H129γ lines were summed together, in view of the obvious difficulty of separating their overlapping profiles. In addition, some observations of the Carina Nebula and G350+0 refer to different compact components, and the treatment of them, together with the analysis of their more complex source geometry, is given in Sections 3*e* and 4*b*.

At low frequencies, an allowance must be made for the possible presence of line emission arising from the interstellar medium, which Gordon *et al.* (1974) have suggested might make a substantial contribution to the apparent H257α nebular emission. To estimate the temperature of such a distributed background component we require either direct measurements at positions near the nebula or a specific model for the surrounding medium. Using the experimental limits obtained by Batty (1976*a*), upper limits to the distributed line emission temperature can be obtained from the thermal continuum sky brightness distribution on the three following assumptions: (i) thermal continuum sky brightness temperatures near the nebulae may be deduced from the thermal maps of Large *et al.* (1961) and Mathewson *et al.* (1962); (ii) the distributed medium has an electron temperature of 6000 K and a line enhancement factor of 3; (iii) any distributed line emission adds directly to the nebular line emission at all frequencies of interest here, owing to the smallness of the continuum optical depth at 408 MHz for each nebula *averaged over the 50′ arc beam* used for the H252α observations. Assumptions (i) and (ii) have been discussed by Batty (1976*a*).

Table 1 lists (column 4) the background continuum thermal antenna temperature T_C^B arising from the interstellar medium near the nebula (listed in column 1, with galactic coordinates given in columns 2 and 3). This was estimated from the thermal maps, scaled to 408 MHz where necessary. The estimated integrated background line emission $\int T_L^B \, dv$ (column 5) calculated from T_C^B was combined with the measured (Batty 1974) line to continuum ratio $\int T_L \, dv / T_c$ (column 6) to provide the corrected value $\left(\int T_L \, dv \right)' / T_C$ given in column 7. The latter values were used subsequently.

Their error limits imply that the background corrections are upper limits. In each case, the resulting line to continuum ratio correction is $<30\%$, except for M17, where it is estimated as being *twice* the observed intensity. Thus, probably the other corrections are also overestimated, but this does not substantially alter the conclusions reached from the susequent analysis. On the basis of these calculations, only the H252α and H257α line data should be measurably affected.

Table 1. Estimated corrections for H252α background line emission

(1) HII region	(2) l (°)	(3) b (°)	(4) T_C^B (K)	(5) $\int T_L^B \, dv$ (K kHz)	(6) $\int T_L \, dv / T_c$ (kHz)	(7) $(\int T_L \, dv)' / T_c$ (kHz)
RCW 38	268·0	−1·1	4·7	2·3	$0{\cdot}28 \pm 0{\cdot}07$	$0{\cdot}26^{+0{\cdot}09}_{-0{\cdot}07}$
RCW 49	284·3	−0·3	28	13	$0{\cdot}21 \pm 0{\cdot}10$	$0{\cdot}15^{+0{\cdot}16}_{-0{\cdot}10}$
Carina Neb. (A)	287·5	−0·5	37	18	$0{\cdot}16 \pm 0{\cdot}02$	$0{\cdot}11^{+0{\cdot}07}_{-0{\cdot}02}$
Carina Neb. (B)	287·8	−1·0	28	13	$0{\cdot}20 \pm 0{\cdot}03$	$0{\cdot}16^{+0{\cdot}07}_{-0{\cdot}03}$
Carina Neb. (C)	287·1	−0·8	28	13	$0{\cdot}23 \pm 0{\cdot}10$	$0{\cdot}16^{+0{\cdot}17}_{-0{\cdot}10}$
G305+0	305·3	+0·2	18	9	$0{\cdot}34 \pm 0{\cdot}04$	$0{\cdot}29^{+0{\cdot}09}_{-0{\cdot}04}$
M17	15·0	−0·7	150	72	$0{\cdot}14 \pm 0{\cdot}05$	$0{\cdot}0\ ^{+0{\cdot}19}_{-0{\cdot}0}$

3. Model Description

(*a*) *General Concepts*

As with most recent models used for the analysis of recombination line data, each HII region is here assumed to be spherically symmetric. In the present analysis, this permits (as a first step) the unique determination of the radial r.m.s. electron density distribution $\langle N_e^2(r) \rangle^{\frac{1}{2}}$ by an appropriate mathematical transformation of the observed radio brightness temperature distribution. A symmetric model also has the desirable property of reducing the computational time and complexity.

The model is assumed to be completely characterized by the electron temperature and density at each point. Since $\langle N_e^2(r) \rangle^{\frac{1}{2}}$ is specified by the continuum data down to essentially the resolution limit of the original map, the only free parameters that may be varied to obtain agreement with the recombination line observations are (i) the electron temperature, assumed to be uniform in most cases, and (ii) the local *fluctuations* in the electron density about the previously determined r.m.s. values which must remain *unchanged.* The magnitude of these fluctuations is assumed to be a simple function of radial distance.

In practice, local density fluctuations (or clumping), which are known from high resolution radio and optical observations to exist in HII regions, have complex and varied structures. Here it is simply assumed that the density fluctuations occur *along* the line of sight and are described by a simple form of distribution, consisting of alternating layers of different density. For the present sources, this simplification produces no serious bias, provided that the correct interpretation is given to the peak densities deduced from the analysis—namely, that they are *lower limits* to the true peak densities in the nebulae.

The integrated line to continuum ratios were calculated for each model, and the free model parameters were then varied to obtain best agreement with the observed ratios. Collisional ('pressure') broadening effects were taken into account. A

baseline subtraction bias, similar to that described by Brocklehurst and Seaton (1972), was assumed to be present in the observational data. For most sources it was possible to obtain a satisfactory fit to the available hydrogen α recombination line data by choosing appropriate model parameters. The computed line widths and higher-order line ratios were then also in reasonable agreement with the observations. The observable line properties of the models appear to fall into relatively independent high and low frequency regimes, which correspond to different physical regions, and it is possible to characterize most of the models by the following three parameters: (i) the electron temperature T_e, assumed to be uniform throughout the nebula (except for RCW 38; see Section 4*b*); (ii) a clumping factor C_{cr} describing the degree of density fluctuation in the core of the nebula; (iii) a similar clumping factor C_{or} for the outer region of the nebula. (The general form of the clumping factor is given in equation (2) below.)

Table 2. Source parameters for single-component models

HII region	Distance (kpc)	5 GHz base level (K)	References for distance
RCW 38	1·0	0·5	Manchester *et al.* (1970); Radhakrishnan *et al.* (1972)
RCW 49	5·0	0·5	Manchester *et al.* (1970); Westerlund (1960)
M17	2·4	0·7	Shaver and Goss (1970)

Table 3. Source parameters for multi-component models

(1) HII region	(2) Source component	(3) N_0 (cm^{-3})	(4) $r_{\frac{1}{2}}$ (pc)	(5) Electron distribution	(6) T_e (K)	(7) Distance (kpc)
Carina Neb.	Outer	31	27	Uniform	8000	2·7[A]
G287·4−0·6	I	235	7·4	Gaussian	8000	2·7[A]
G287·6−0·6	II	247	6·7	Gaussian	8000	2·7[A]
G305+0	Outer	12	41	Uniform	5000	8·0[B]
G305·4+0·2	I	265	9·2	Gaussian	5000	8·0[B]
G305·2+0·2	II	102	19·1	Gaussian	5000	8·0[B]
G305·2+0·0	III	141	12·5	Gaussian	5000	8·0[B]

[A] Distance measurement from Sher (1965).
[B] Distance measurement from Wilson *et al.* (1970) and Goss *et al.* (1972).

(*b*) *Derivation of Density Distributions*

For a spherically symmetric nebula, the square of the radial r.m.s. electron density distribution and the observed variation in emission measure across its face as seen by a distant observer are related by the following form of the Abel transform (Wade 1959; Bracewell 1965):

$$N_e^2(r) = -\frac{1}{\pi}\int_r^\infty \frac{\mathrm{d}E(x)/\mathrm{d}x}{(x^2-r^2)^{\frac{1}{2}}}\,\mathrm{d}x, \tag{1}$$

where r is the radial distance from the centre of the nebula, x is the projected radial distance normal to the line of sight and $E(x)$ is the projected radial distribution of emission measure.

For RCW 38, RCW 49 and M17, an examination of the 5 GHz maps of Shaver and Goss (1970), made with a 4′ arc beam, indicates that the approximation of spherical symmetry is reasonable, and these sources were analysed in the following manner: A beam deconvolution was applied to the maps and, since the brightness profile could be approximated very closely by a central gaussian peak added to an extended source, the deconvolution was more conviently applied separately to these components. The function $\langle N_e^2(r)\rangle^{\frac{1}{2}}$ was then obtained from equation (1) by using values of $E(x)$ calculated on the assumption of a small optical depth at 5 GHz and for the parameter values given in Table 2. The derived densities are weakly dependent on the assumed value for T_e, which was initially taken to be 7000 K. In subsequent calculations involving different values of T_e, the dependence on electron temperature was allowed for, and the electron densities were rescaled slightly to compensate. The radial electron density distributions required to produce the observed brightness profiles for RCW 38, RCW 49 and M17 are shown in Fig. 1.

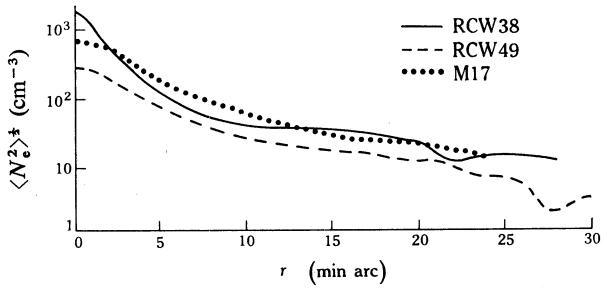

Fig. 1. Computed radial distributions of the r.m.s. electron density $\langle N_e^2\rangle^{\frac{1}{2}}$ for spherically symmetric models of the indicated HII regions. An angular displacement of 1′ arc corresponds to linear distances of 0·29, 1·46 and 0·70 pc for RCW 38, RCW 49 and M17 respectively.

The Carina Nebula and G305+0 have more complex structures than the other HII regions considered here, and the assumption of spherical symmetry cannot be used for them. For these sources, the emission was divided into an extended low density component (labelled 'outer' in column 2 of Table 3), and two or more higher density 'cores' corresponding to the strongest peaks (labelled I, II, ... in column 2 of Table 3). The properties of the core components were taken from Shaver and Goss (1970), except that a gaussian electron density profile has been assumed ('gaussian' distribution in column 5 of Table 3) and the density values have been rescaled accordingly. The flux density of the outer component was estimated from the residual integrated flux density for the nebula after subtraction of the core components, its electron density profile being assumed to be constant ('uniform' distribution in column 5 of Table 3). Thus, for both sources, some of the minor components were lumped with the extended outer component. Parameter values for each source component are also listed in Table 3. Column 3 gives its central electron density N_0, column 4 gives its radius $r_{\frac{1}{2}}$ to half-peak density, column 6 gives the electron temperature T_e and column 7 gives the distance to the HII region.

(c) Calculation of Line and Continuum Intensities

This subsection outlines the computational procedures used in the model calculations, a more detailed account having been given elsewhere (Batty 1976*b*). The

spherically symmetric electron density distributions were obtained as described in the previous subsection. The observable line profiles were then computed by integrating the equation of transfer along regularly spaced lines of sight for a range of points across each profile. The Voigt function for each integration step was evaluated using the approximations of Whiting (1968). The effects of beam smoothing were simulated by weighting the results, assuming a gaussian antenna beam of specified size centred on the nebula.

In order to introduce density variations along the line of sight, the integration was performed in steps alternating between two values of electron density (i.e. for a series of thin homogeneous layers). These values were continuously varied along the line of sight so that the local average values of the r.m.s. density were preserved. A local clumping factor C was defined by

$$C(r) = \frac{\langle N_e \rangle_E}{\langle N_e^2 \rangle^{\frac{1}{2}}} \equiv \frac{\int N_e^3 \, ds \,/\, \int N_e^2 ds}{\left(\int N_e^2 \, ds \right)^{\frac{1}{2}}}, \tag{2}$$

where the averages are taken over a local region rather than along the whole line of sight s (cf. Hjellming *et al.* 1969). The local clumping factor was taken to be a function of radial distance only. Calculations indicate that the line properties of the model are relatively insensitive to the specific clumping amplitude distribution used; they depend almost entirely on $\langle N_e \rangle_E$ (essentially a measure of the clump density) and T_e.

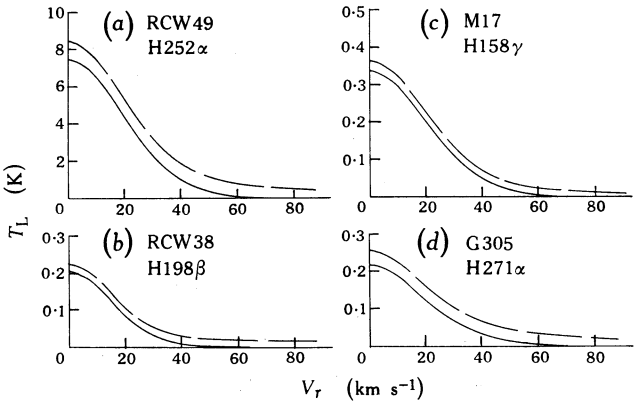

Fig. 2. Computed line profiles showing the variation of the specified line temperature T_L as a function of the radial velocity V_r for the indicated HII regions. The original profiles are given as dashed curves, while the same profiles, after baseline removal, are given as full curves.

In order to compare the calculated results with observation it was assumed that a baseline subtraction effect occurs in the reduction of observational data, as described by Brocklehurst and Seaton (1972). Large collisional broadening effects tend to redistribute the line energy into broad wings. These wings are assumed to be subtracted when baseline corrections are made by fitting a smooth function (usually a polynomial) away from the line centre. In the present calculations the function

$$F(v) = A - B(v - v_0)^2 \tag{3}$$

(where v is the frequency, v_0 is the line centre frequency, and A and B are constants) was fitted out to ~ 90 km s^{-1} from the line centre, and gave a good fit to the line wings. Fig. 2 shows some typical computed line profiles before (dashed curves) and after (full curves) baseline removal. A baseline correction factor ξ was defined by

$$\xi \equiv \left(\int T_L \, dv\right)_{BS} / \int T_L \, dv, \tag{4}$$

where the subscript BS denotes that baseline subtraction has been performed.

Lockman and Brown (1975) have questioned the above techniques, suggesting that the resulting correction factors are arbitrary. While it is clear that the methods of estimating baseline confusion effects are far from ideal (since the procedure used by observers varies), it is considered that these results should not be seriously in error. In almost all the profiles computed here, the gaussian-like cores were usually well defined and the wings were shallow. The fitted baselines agreed well with those estimated by eye, and the resultant line intensities should not be in error by more than $\sim 5\%$–10%, which is comparable with the accuracy of the observations. In a few cases only, where the calculated profiles had very steep wings (e.g. for some higher order lines in M17), it was apparent that *any* procedure would be unreliable for the practical estimation of line parameters, even if a baseline were not removed.

(d) Clumping Structure Approximation

The exclusion of clumping effects normal to the line of sight (i.e. treating the clumping as a series of thin layers, each lying across the line of sight) produces possible biases, which should be understood when assessing the models:

(i) In any real nebula the true maximum values of the continuum optical depth will always be greater than in the models whenever fine structure (which may be considered as clumping normal to the line of sight) is present. Over the range of most line observations ($v \lesssim 5$ GHz), the continuum optical depth contributes significantly to the line enhancement. For example, the expression for the line enhancement factor Y in a constant density region (Brocklehurst and Seaton 1972) is

$$Y = b\left\{\frac{\tau}{\exp(\tau)-1} + (1-\beta)\left(1 - \frac{\tau}{\exp(\tau)-1}\right)\right\}, \tag{5}$$

where b is the departure coefficient, τ is the continuum optical depth and β is a stimulated emission factor. For a constant electron temperature, the line enhancement thus depends on two factors: higher values of τ lead to increased line enhancement; the net effect of increasing the electron density is to diminish the apparent line intensity (both by restoring $1-\beta$ to unity and by increasing collisional broadening). Line intensities calculated from a model having low τ values, but using the *true* peak electron densities in the nebula, will be lower than those observed. Agreement with the line observations is only obtained if the peak densities in the model are lowered. This implies that the densities fitted in the analysis should be regarded as *lower limits* to the true peak nebular densities.

(ii) The models will not accurately reproduce the observed continuum spectrum when the optical depth through the compact components is appreciable. For example, the models of RCW 38 and M17 (which have the highest central emission measures) overestimate the 408 MHz continuum flux densities by $\sim 35\%$ and $\sim 21\%$ respectively. This effect, which was allowed for in the low frequency calculations, becomes rapidly insignificant at higher frequencies; it does not affect the general conclusions.

(iii) In order to simplify the clumping parameters, each model was divided into a core and an outer region, the boundary lying at a radius equal to the full half-brightness width of the central distribution. The clumping factor was assumed to have independent values C_{cr} and C_{or} in these two regions. This simply provided a convenient method of separating clumping effects in the dense core from those in the less dense outer regions. It was found that for $n \lesssim 160$ the α line solutions depended primarily on C_{cr}, while for $n \gtrsim 200$ they depended primarily on C_{or}.

It is possible that a separation of the solutions into low and high frequency regimes may not be valid if clumping normal to the line of sight is included. The high frequency line properties of the core will be relatively unaffected by changes in the properties of the outer low density gas, since the latter contributes little to the high frequency line or continuum radiation. However, the properties of the core are important in determining the low frequency line behaviour of the model, even when the line radiation from the core is highly collisionally broadened and undetectable. This is because the strong continuum radiation from the core is very effective in producing maser action in the lower density foreground gas. If the source of this continuum is spatially modified by clumping normal to the line of sight, the resulting line intensity will change.

After consideration of the above effects on the present models, it was concluded that no serious bias occurs. At low frequencies, the apparent line radiation along the central line of sight (as seen with small beamwidths) is due almost entirely to maser action in the foreground gas produced by the 'background' continuum from the core, and should be proportional to the background intensity at each position. The *average* line emission over this region should thus be proportional to the *average* 'background' brightness temperature, independent of its spatial distribution, and thus the observed line to continuum ratio should be independent of the spatial clumping in the core. In addition, with large beamwidths at low frequencies (the usual case), most of the observed line and continuum radiation may be produced in the outer regions and hence also be independent of the spatial structure of the core. But this clearly depends on the individual source.

To examine these effects, a model consisting of a gaussian clump embedded in a low density ($50\ \mathrm{cm}^{-3}$) outer region was considered. The diameters of the clump and outer region were taken to be 4′ and 25′ arc respectively, while the electron temperature was taken to be 8000 K. The emission measure through the centre of the outer component was taken to be $\sim 2 \times 10^4\ \mathrm{pc\,cm}^{-6}$. A range of clump densities was then considered, and gave central emission measures of $\sim 3 \times 10^5$ to $\sim 6 \times 10^6\ \mathrm{pc\,cm}^{-6}$, representative of the sources of interest here. The clump diameter was then reduced to 2′ arc, so that the solid angle subtended by the core was reduced by a factor of 4.

At the same time, the core density was scaled up to maintain the 5 GHz flux density constant. For a given observed flux density, this simulated the effects of clumping both along and normal to the line of sight. The H252α line intensities (corrected for baseline removal) were calculated for observational beamwidths of 50′ and 2′ arc. After 'clumping', the change in the H252α line to continuum ratio was $<15\%$ and $<5\%$ respectively for the two beamwidths, although the latter was rather sensitive to the baseline removal procedure. This difference is comparable with the observational errors. Thus, for the purposes of the present analysis, the solutions for the core and outer regions may be considered to be relatively independent.

(*e*) *Fitting Procedures*

A fitting was initially made *only* to the available hydrogen α line to continuum ratios, taking into account baseline subtraction. The observational half-power beamwidth $\theta_{\frac{1}{2}}$ was assumed to be given by

$$\theta_{\frac{1}{2}} = 20/\nu_0 \quad \text{min arc} \tag{6}$$

(with ν_0 in GHz) for all α line and for M17 β line calculations; in other cases, the actual observational beamwidth was used.

Table 4. Fitted model parameters

(1) HII region	(2) Model designation	(3) T_e (K)	(4) C_{cr}	(5) C_{or}†	(6) N_e^P (cm^{-3})	(7) Notes
RCW 38	D	7000	15	1	$\geqslant 2{\cdot}5\times10^4$	$T_e \leqslant 4000$ K in outer region
RCW 49	C	6500	30	3	$\geqslant 9\times10^3$	—
Carina Neb.	C–E	7000(?)	7(?)	3	$\geqslant 1{\cdot}8\times10^3$	Confusing fit to data
G305+0	C	5000	$\leqslant 3$	4	$\geqslant 8\times10^2$	High frequency data for G305·4+0·2 only
M17	C	7300	3	10	$\geqslant 2{\cdot}1\times10^3$	—

† For RCW 38, $C_{or} = 1$ if $T_e = 4000$ K for the outer region. If the outer region is cooler, C_{or} must be increased.

Using an initial estimate of T_e, the α line calculations were made for each source, assuming no clumping ($C_{cr} = C_{or} = 1$) for both LTE and non-LTE cases (referred to as models A and B respectively for each source). These represent two extreme cases. As C is increased, the line intensities tend to those for model A if collisional broadening is ignored. Conversely, model B represents the maximum possible deviation from model A, given the other model constraints. By comparing these two models with the data, a choice of free parameters could be made to optimize the fit, taking into account the baseline correction factors. No model alterations were made to obtain agreement with observed line widths, although the agreement of higher-order line data was examined and, in one case (RCW 38), this was taken into account to slightly improve the fit.

A modified procedure was used for both the Carina Nebula and G305+0 due to their complex geometry. In their case, most of the high frequency line observations are of one or more of the smaller components, which may be analysed in the previous manner, while the H252α observations include almost all of the components. For

the latter, the individual contributions to the observed line and continuum emission may be summed, since the various components lie along different lines of sight. For each nebula, calculations were made separately for the low density outer component and then for an identical region having each compact component added in turn to the centre of the model. The intensities were then combined appropriately.

4. Results

(*a*) *Numerical Results*

Table 4 summarizes the best fitted parameter values for T_e, C_{cr}, C_{or} and N_e^P (the peak electron density) in columns 3–6 for the model types given in column 2. The model types are defined in the captions to Figs 3 and 4. Comparisons between the observed and calculated line to continuum ratios for various higher-order hydrogen line transitions are listed in Table 5. Figs 3 and 4 show comparisons between observed and calculated α and β (M17 only) line intensities as a function of the principal quantum number n.

Table 5. Comparison of data for higher-order transitions in hydrogen

HII regions	Transition	$(\int T_L \, dv/T_c)_{obs}$ (kHz)	$(\int T_L \, dv/T_c)_{calc}$[A] (kHz)	ξ
RCW 38	H137β	4·22±0·45	4·46	0·61
RCW 38	H198β	0·33±0·25	0·32	0·38
RCW 38	H(113β+129γ)	14·9 ±(≥30%)	27·0	0·80
RCW 49	H137β	4·19±0·76	5·44	0·71
RCW 49	H198β	<0·24±0·21	0·29	0·35
Car I	H137β	6·13±1·14	6·51	0·91
Car(I+II)	H198β	<0·30±0·27	0·48	0·62
Car I	H(113β+129γ)	29±(≥20%)	32·4	0·95
M17	H(113β+129γ)	27·1 ±(≥15%)	28·8	0·86
M17	H157γ	2·45±0·6	2·45	0·76
M17	H158γ	2·93±0·27	2·34	0·76
M17	H225γ	0·36±0·17	0·27	0·79
M17	H241γ	0·21±0·05 (Voigt) 0·14±0·03 (Gaussian)	0·053	0·15
M17	H173δ	1·57±0·14	1·14	0·64
M17	H186ε	0·82±0·14	0·51	0·45

[A] The calculated line to continuum data have been corrected for baseline subtraction effects.

The accuracy of the fitted parameters (Table 4) is difficult to define because the peak density estimates are lower limits. In general, uncertainties of $\sim 10\%$ in T_e and $\lesssim 30\%$ in the C values are probably realistic. In a few cases, where a problem in fitting individual data was noted, these estimates must necessarily be raised. Fig. 5 shows the calculated α linewidths ΔV_L as a function of the principal quantum number n. The resulting ratios of H252α to H109α widths† (after baseline subtraction) agree with those measured by Batty (1974). In most cases this merely indicates that no significant collisional broadening is detectable at these frequencies, as the effect is relatively small, and effects due to multiple Doppler components may be present.

† More correctly, the widths of the best fit gaussians should be used, but the difference is small in the present case.

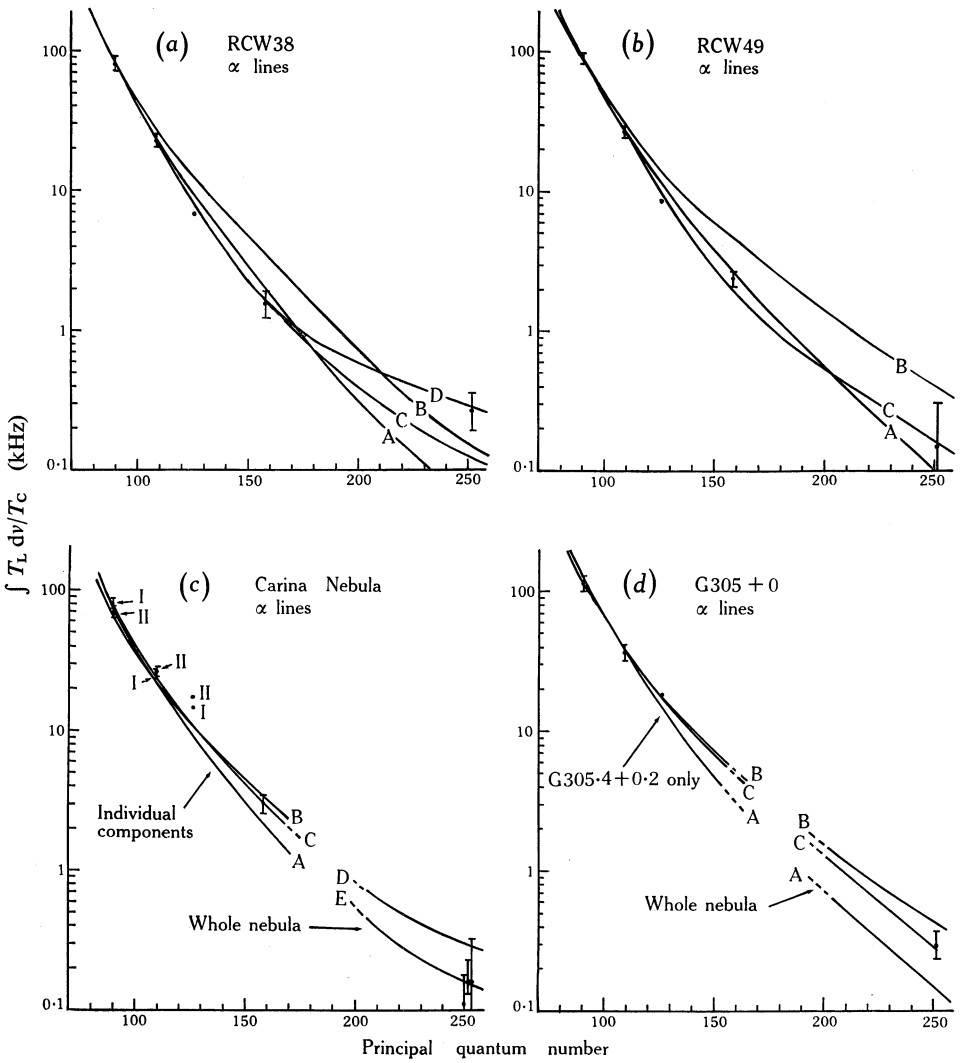

Fig. 3. Comparison between the observed (points) and calculated (curves) α line to continuum ratios $\int T_L \, dv/T_C$ for the indicated HII regions.

(*a*) *RCW 38.* Models used are: A, LTE with $T_e = 7500$ K; B, smooth non-LTE with $T_e = 7500$ K; C, clumped non-LTE with $T_e = 7000$ K; D, clumped non-LTE with $T_e = 7000$ K (core) and 4000 K (outer region).

(*b*) *RCW 49.* Models used are: A, LTE with $T_e = 7000$ K; B, smooth non-LTE with $T_e = 7000$ K; C, clumped non-LTE with $T_e = 6500$ K.

(*c*) *Carina Nebula.* Models used are: A, LTE with $T_e = 8000$ K; B–D, smooth non-LTE with $T_e = 8000$ K; C–E, clumped non-LTE with $T_e = 7000$ K. For $n \leqslant 160$ the calculations are for the two main components (I and II as indicated), while for $n \geqslant 200$ the calculations include all components.

(*d*) *G305+0.* Models used are: A, LTE with $T_e = 5000$ K; B, smooth non-LTE with $T_e = 5000$ K; C, clumped non-LTE with $T_e = 5000$ K. For $n \leqslant 160$ the calculations are for component I (G305·4+0·2), while for $n \geqslant 200$ the calculations include all components.

The effects of baseline removal have been included in the calculations.

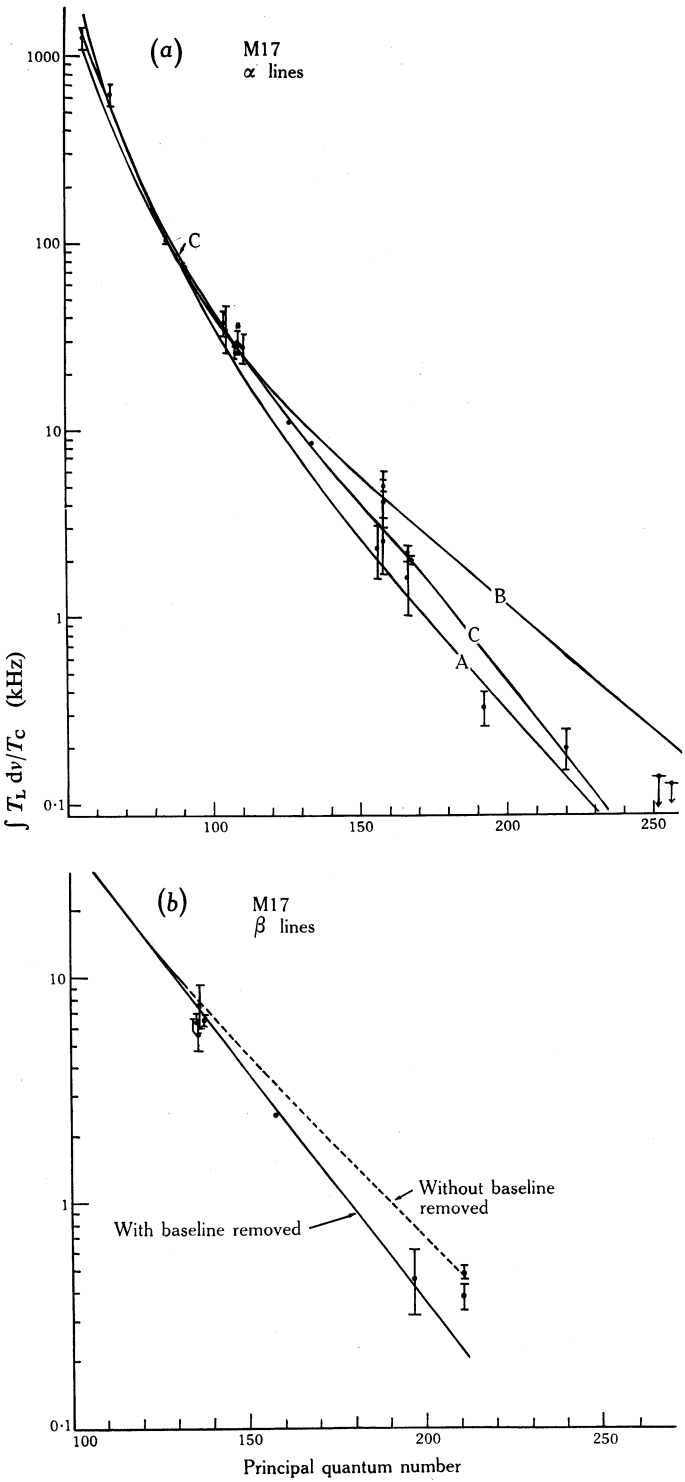

Fig. 4 *(See caption on opposite page)*

(b) Individual Models

(i) *RCW38.* The fitted central temperature of 7000 K for RCW 38 is consistent with the estimate of 7500 K made by Shaver and Goss (1970), but a lower outer temperature of $\leqslant$4000 K was required to obtain agreement with H252α data (see Fig. 3*a*). This is in accordance with Shaver's (1970) temperature estimate of 4000$\pm$2000 K obtained from 85 MHz data, and with the estimate of 6000$\pm$2600 K made by Wilson *et al.* (1970) for the extended component G267·8$-$0·9. There is thus clear evidence for a radially decreasing temperature in the nebula. The H126α and H158α data points are both depressed below the LTE solutions (in spite of a net line enhancement) due to a high degree of collisional broadening in the dense core.

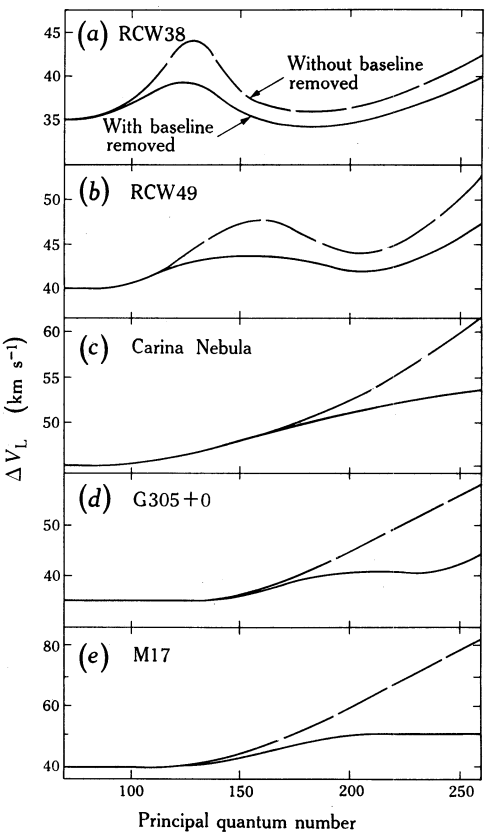

Fig. 5. Calculated half-power α linewidths ΔV_L plotted as a function of the principal quantum number for source models fitted to the indicated HII regions. The minimum linewidths correspond to the adopted Doppler widths for the sources. The effects of baseline removal are apparent from a comparison between the relations before (dashed curves) and after (full curves) baseline removal.

Fig. 4 (*opposite*). Comparison between the observed (points) and calculated (curves) line to continuum ratios for M17.

(*a*) α *line data.* Models used are: A, LTE with T_e = 8000 K; B, smooth non-LTE with T_e = 8000 K; C, clumped non-LTE with T_e = 7300 K. The effects of baseline removal have been included in the calculations.

(*b*) β *line data.* Model used is: C, clumped non-LTE with T_e = 7300 K. The effects of baseline removal are indicated. Observational beamwidths given by equation (6) have been assumed.

The higher-order line data agree reasonably well with the model, except for the H($113\beta+129\gamma$) point, but an examination of the original data indicate the possibility of additional baseline uncertainties near these transitions. The non-monotonic variation of the α linewidth with the principal quantum number (Fig. 5*a*) is due to an interaction between collisional broadening and source-geometry effects as the beam size and quantum number vary.

(ii) *RCW49.* Shaver (1970) and Shaver and Goss (1970) obtained continuum-based estimates for the electron temperature of RCW 49 of 6000 ± 2000 K and 7750 K respectively, which are reasonably consistent with the fitted value of 6500 K. The H126α and H158α data points (see Fig. 3*b*) exhibit the same depression as for RCW 38, while the agreement for the few higher-order data points is satisfactory. An interesting feature is the very low value of ξ for H198β, which leads to high values ($>10^4$ K) for the electron temperature T_e^* calculated under LTE assumptions. This implies that, as for RCW 38, the limiting value of T_e^* derived from higher-order lines near the same frequency may not necessarily be a good approximation to the true electron temperature, as has often been assumed. For different order lines near the same frequency, the principal quantum number increases with the line order, causing the collisional broadening effects to increase rapidly (the ratio of collisional to Doppler widths varies as $\sim n^{7\cdot4}$). As a result, ξ decreases with increasing line order, and the successive values of T_e^* thus derived do not necessarily converge, unless ξ is close to 1.

(iii) *Carina Nebula.* Radio continuum and optical determinations of the temperature of the Carina Nebula range from $\sim$8000–10 000 K (Faulkner and Aller 1965; Shaver 1970; Shaver and Goss 1970). A temperature estimate is difficult to obtain from the line data. The model calculations shown in Fig. 3*c* hold only for components I and II (as indicated) for $n \leqslant 160$, but for the whole nebula for $n \geqslant 200$. A composite model (labelled C–E) consisting of model C for the low-n regime and model E for the high-n regime, and with $T_e = 7000$ K and $C_{cr} = 7$,† fits the high frequency data except for the H126α points. On the other hand, a model with $T_e = 5000$ K and $C_{cr} = 1$ fits all but the H158α data. For an isothermal model, agreement with all data points cannot be obtained, and so any solution is tentative. In any case, a central temperature of $\sim$10 000 K does *not* appear to be consistent with the line data. Shaver's (1970) determination of 10 000 K from 85 MHz data could be explained by a radial temperature gradient, but this is not the case for the optical temperatures, which refer to more compact components. It is likely that a more complex temperature structure exists and that observational selection effects have occurred. The variations in T_e^*(H109α) measured by Gardner *et al.* (1970*a*) support this view, but more confirming data are needed, and α line measurements near $n = 140$ may be useful. For the C–E model, the agreement with the higher-order line data is quite good.

(iv) *G305+0.* The fitted temperature of 5000 K for G305+0 agrees with the value of 4000 ± 2000 K obtained by Shaver (1970), although it is slightly higher than the determinations by Shaver and Goss (1970) of 3350 and 3750 K for the main components. Since the H90α data (R. X. McGee, personal communication) refer only to component I in Table 3 (G305·4+0·2), and since the H109α line to continuum

† Due to the similarity of their observed properties, the same value of C_{cr} was assumed for both components.

ratios are similar for the main components, an analysis for G305·4+0·2 only was attempted using the high frequency data. The value of C_{cr} was rather poorly determined by the model fit.

(v) *M17.* The nebula M17 has been the subject of numerous line and continuum studies. Radio continuum and optical temperature determinations give values in the range ~7000–8500 K (e.g. Peimbert and Costero 1969; Shaver 1970; Shaver and Goss 1970), while Hjellming and Gordon (1971) found a best solution of 7500±800 K from a recombination line analysis. The value of 7300 K deduced here appears consistent with most of these data. The agreement with the available higher-order line data is reasonably good but appears to worsen as the line order is increased. Notable discrepancies occur with the H211β data (although the observational baseline is poor) and the H241γ, H173δ and H186ε data. The computed H225γ and H241γ profiles have very steep wings, and the validity of baseline subtraction procedures for these lines is very questionable. If the computed higher-order line intensities are too low, as the fit suggests, this would imply a lower temperature or lower peak density, or a higher central optical depth. The latter seems to be the most likely, and the bias is probably a result of neglecting clumping normal to the line of sight. This is also suggested by the fact that the analysis of Hjellming and Gordon (1971) yields a peak density which is an order of magnitude higher than that fitted here and which is also in general agreement with values deduced from aperture synthesis observations of the most compact components (Webster *et al.* 1971).

5. Conclusions

For the central parts of the HII regions studied here, electron temperatures in the range ~5000–7300 K are required in the models in order to fit the recombination line data. For most nebulae, these values agree with independent temperature estimates (principally those derived from radio continuum measurements) to within ~1000–1500 K. For the Carina Nebula, however, both the fit to the recombination line data and the discrepancy between the various temperature estimates are confusing, which implies that large temperature variations may be present.

Significant clumping of the gas in the core of the models is usually required to explain the line data, as models with $C_{cr} = 1$ predict line intensities which are generally too high. Best fits to the data are obtained for C_{cr} values in the range ~3–30, indicating peak electron densities at least as high as $\sim 1\text{–}2 \times 10^4$ cm^{-3} in some nebulae. With this degree of clumping, higher resolution radio continuum observations should reveal the presence of finer structure. The only significantly higher resolution studies of the more southern nebulae (excluding M17) have been made with the Fleurs synthesis telescope at 1·4 GHz (Christiansen 1973). Unpublished maps of these regions generally show the presence of more compact components, except in RCW 38, where the central optical depth is >1 at 1·4 GHz, and higher frequency data are required.

The gas in the outer regions of the nebulae also appears to be clumped, although to a lesser extent on average. Values for C_{or} in the range ~3–10 generally give best fits to the data. Alternatively, higher outer temperatures might explain the low frequency line observations, and would be difficult to detect. Lockman and Brown (1975) suggested that a radially increasing temperature is required to explain line intensities in the Orion Nebula; however, no evidence to support this conclusion is available for the present nebulae, while for RCW 38 the converse appears to hold.

The model of RCW 38 requires a lower temperature ($\leqslant 4000$ K) outer region in order to explain the observed H252α line intensity. This agrees with temperature determinations of the outer component made independently by other methods. It is interesting to note that the presence of a low temperature outer region, not a readily observable feature of thermal sources, might often be detectable by means of low frequency recombination line measurements. For example, Pankonin (1973) has deduced a similar result for W49A from the widths of the H247α/H248α lines.

For the models of RCW 38 and RCW 49, the values of electron temperature T_e^* derived from the calculated line to continuum ratios under LTE assumptions do *not* converge to the actual model temperature as the line order is increased near $\nu = 1{\cdot}7$ GHz. Instead, collisional broadening effects cause the baseline correction factor ξ to decrease rapidly for higher-order transitions, thus biasing T_e^* toward higher values. Note that this result was obtained independently of the observations, and depends on the individual model structure only. Thus, although this traditional method of estimating electron temperatures may yield meaningful results for some nebulae and/or transitions (see e.g. Brocklehurst and Seaton 1972), it must generally be used with caution in the analysis of experimental data.

A more realistic estimate of clumping effects (and hence of peak densities) in HII regions should be possible if better models of the clumps are considered. In particular, the inclusion of clumping normal to the line of sight could be made. In this type of model, the effective 'area covering factor' depends on the relative size, shape and spatial arrangement of the clumps, and is not easily determined. Salem and Seaton (1974) have considered the determination of this quantity in conjunction with continuum models of HII regions, and similar parameters might be estimated from a detailed examination of the continuum spectra for different regions of a source. In addition, local densities derived from optical line ratio measurements may help to define the models. However, for most of the sources studied here, it is probable that the relative paucity of available recombination line data would preclude the use of a much more complex modelling scheme at the present time.

Acknowledgments

It is a pleasure to thank Dr R. X. McGee for providing data prior to publication, Dr W. M. Goss and Dr A. J. Turtle for helpful discussions, and Dr T. B. H. Kuiper and Dr S. Gulkis for useful manuscript criticisms. This work was carried out while the author was a postgraduate student in the Chatterton Astrophysics Department, University of Sydney, where research is supported by the Australian Research Grants Committee, the Sydney University Research Grants Committee and the Science Foundation for Physics within the University of Sydney.

References

Batty, M. J. (1974). *Mon. Not. R. Astron. Soc.* **168**, 37P.

Batty, M. J. (1976*a*). *Aust. J. Phys.* **29**, 419.

Batty, M. J. (1976*b*). Ph.D. Thesis, University of Sydney.

Bracewell, R. M. (1965). 'The Fourier Transform and its Applications', p. 262 (McGraw-Hill: New York).

Brocklehurst, M., and Seaton, M. J. (1972). *Mon. Not. R. Astron. Soc.* **157**, 179.

Cato, B. T. (1973). Research Electronics Laboratory, Onsala Space Observatory, Chalmers University, Tech. Res. Rep. No. 114.

Christiansen, W. N. (1973). *Proc. Inst. Radio Electron. Eng. Aust.* **34**, 302.
Faulkner, D. J., and Aller, L. H. (1965). *Mon. Not. R. Astron. Soc.* **130**, 393.
Gardner, F. F., Milne, D. K., Mezger, P. G., and Wilson, T. L. (1970*a*). *Astrophys. Lett.* **6**, 87.
Gardner, F. F., Milne, D. K., Mezger, P. G., and Wilson, T. L. (1970*b*). *Astron. Astrophys.* **7**, 349.
Gordon, K. J., Gordon, C. P., and Lockman, F. J. (1974). *Astrophys. J.* **192**, 337.
Goss, W. M., Radhakrishnan, V., Brooks, J. W., and Murray, J. D. (1972). *Astrophys. J. Suppl.* No. 203, 123.
Hjellming, R. M., Andrews, M. H., and Sejnowski, T. J. (1969). *Astrophys. J.* **157**, 573.
Hjellming, R. M., and Gordon, M. A. (1971). *Astrophys. J.* **164**, 47.
Huchtmeier, W. K. (1974). *Astron. Astrophys.* **32**, 335.
Large, M. I., Mathewson, D. S., and Haslam, C. G. T. (1961). *Mon. Not. R. Astron. Soc.* **123**, 113.
Lockman, F. J., and Brown, R. L. (1975). *Astrophys. J.* **201**, 134.
McGee, R. X., Batchelor, R. A., Brooks, J. W., and Sinclair, M. W. (1969). *Aust. J. Phys.* **22**, 631.
McGee, R. X., and Gardner, F. F. (1968). *Aust. J. Phys.* **21**, 149.
McGee, R. X., Newton, L. M., and Batchelor, R. A. (1975). *Aust. J. Phys.* **28**, 185.
Manchester, R. N., Robinson, B. J., and Goss, W. M. (1970). *Aust. J. Phys.* **23**, 751.
Mathewson, D. S., Healey, J. R., and Rome, J. M. (1962). *Aust. J. Phys.* **15**, 354.
Pankonin, V. L. (1973). Ph.D. Thesis, Cornell University.
Pedlar, A., and Davies, R. D. (1972). *Mon. Not. R. Astron. Soc.* **159**, 129.
Peimbert, M., and Costero, R. (1969). *Bull. Tonantzintla Tacubaya Obs.* **5**, 3.
Radhakrishnan, V., Goss, W. M., Murray, J. D., and Brooks, J. W. (1972). *Astrophys. J. Suppl. Ser.* No. 203, 49.
Salem, M., and Seaton, M. J. (1974). *Mon. Not. R. Astron. Soc.* **167**, 493.
Shaver, P. A. (1970). *Astrophys. Lett.* **5**, 167.
Shaver, P. A., and Goss, W. M. (1970). *Aust. J. Phys. Astrophys. Suppl.* No. 14, 133.
Sher, D. (1965). *Q. J. R. Astron. Soc.* **6**, 299.
Simpson, J. P. (1970). Ph.D. Thesis, University of California.
Wade, C. M. (1959). *Aust. J. Phys.* **12**, 418.
Waltman, E. B., and Johnston, K. J. (1973). *Astrophys. J.* **182**, 489.
Webster, W. J., Altenhoff, W. J., and Wink, J. E. (1971). *Astron. J.* **76**, 677.
Westerlund, B. E. (1960). *Ark. Astron.* **2**, 419.
Whiting, E. E. (1968). *J. Quant. Spectrosc. Radiat. Transfer* **8**, 1379.
Wilson, T. L., Mezger, P. G., Gardner, F. F., and Milne, D. K. (1970). *Astron. Astrophys.* **6**, 364.

Manuscript received 1 September 1976, revised 24 July 1978